Journal of Applied Polymer Science

Copper Hexacyanoferrate–Polymer Composite Beads for Cesium Ion Removal: Synthesis, Characterization, Sorption, and Kinetic Studies

Charu Dwivedi,[1] Amar Kumar,[2] Krishan Kant Singh,[1] Ajish K. Juby,[1] Manmohan Kumar,[1] Piaray Kishen Wattal,[2] Parma Nand Bajaj[1]

[1]Radiation and Photochemistry Division, Bhabha Atomic Research Centre, Trombay, Mumbai 400085, India
[2]Process Development Division, Bhabha Atomic Research Centre, Trombay, Mumbai 400085, India
Correspondence to: M. Kumar (E-mail: manmoku@barc.gov.in)

ABSTRACT: A novel synthetic method for the preparation of different sorbent–polymer composite beads has been developed under simple laboratory conditions. Copper hexacyanoferrate was synthesized, and its composite beads of required size were synthesized by phase-inversion technique, using polyethersulfone as the polymer matrix. Suitable size and mechanical stability, along with their spherical shape, make these composite beads most appropriate for column operation. The efficiency of these composite beads was tested for the removal of cesium, using radioanalytical techniques, in batch conditions. The effect of pH, the initial metal ion concentration, and contact time was also investigated. The synthesized beads perform best in the pH range 5–9. Different sorption isotherm models were applied to the experimental data. Equilibrium data are represented well by the Langmuir isotherm equation, with a monolayer sorption capacity of 1.56 mg g^{-1} for the swollen beads. Kinetic modeling analysis, by fitting the data in the pseudo first-order, pseudo second-order, and intraparticle diffusion equations, shows that the pseudo second-order equation is the most appropriate model for the description of sorption of cesium ions onto the composite beads. The process mechanism is found to be complex, consisting of both intraparticle diffusion and film diffusion. © 2012 Wiley Periodicals, Inc. J. Appl. Polym. Sci. 129: 152–160, 2013

KEYWORDS: separation techniques; applications; composites; functionalization of polymers; adsorption

Received 26 June 2012; accepted 12 October 2012; published online 4 November 2012
DOI: 10.1002/app.38707

INTRODUCTION

Among the operational techniques in water and wastewater treatment, sorption has been proved to be an excellent way to treat industrial waste effluents, offering significant advantages, like the low cost, availability, profitability, easy operation, and efficiency. Several materials, such as activated carbon,[1] chelating resins,[2] clays,[3] and functionalized silica,[4] have been studied for the removal of toxic metal ions from aqueous solutions. Most of the commercialized sorbents are organic resins, having their own limitations, such as poor thermal and radiation stability and mechanical strength. Inorganic sorbents have high chemical and radiation stability, but because of their fine morphology, or gel-like nature, these create excessive pressure drops across the fix bed and low-hydraulic conductivity, and hence, cannot be used as such in any flow-through system.[5] The above-mentioned limitations of the organic resins and the inorganic sorbents can be overcome by introducing composite resins, consisting of inorganic sorbents and organic-binding matrices.

Cesium-137 is one of the important fission fragments present in significant amounts in the radioactive wastes. Its removal from radioactive waste is very important, because it has high radiotoxicity, long half-life ($T_{1/2}$ = 32 years), and high mobility in the biosphere. Many organic and inorganic sorbents are available for the removal of cesium ions from the waste solution, but the advantage of inorganic sorbents is that these have better thermal, chemical, and radiation stability, and mechanical strength. Moreover, after their effective use, these can be easily solidified for the ultimate disposal. In the literature, a considerable number of reports are available on the use of synthetic inorganic sorbents, which have a strong affinity for one or more radionuclides over a wide pH range. The major classes of inorganic ion exchange materials include aluminosilicates,[6] phosphates,[7] ferrocyanides, and hydrous oxides of multivalent cations.[8–10] Among these, hexacyanoferrate complexes have emerged as highly selective ion exchangers for cesium ions.[11–14] These complexes are also used as precipitating agents for cesium ions in nuclear waste. But, their use as ion exchangers is preferred over that as precipitating agents, as the latter give a

Additional Supporting Information may be found in the online version of this article.

colloidal sludge, which is hard to remove. Copper hexacyanoferrate (CuHCF) is available in granular form, but its efficiency in the column operation decreases due to its poor mechanical properties, which leads to the disintegration of the grains and clogging of the bed.[15] Here, we have developed a technique to synthesize a sorbent–polymer composite, containing potential inorganic sorbent, CuHCF, and polyethersulfone (PES) as a binding matrix, for the removal of radioactive cesium ions from low-level nuclear waste.

EXPERIMENTAL

Materials

PES (Gafone PES 3200P) was procured from Gharda Chemicals, India. Polyvinyl alcohol (PVA; molecular weight 1,25,000) was purchased from SD Fine Chemicals, India. Cesium nitrate (99%), potassium hexacyanoferrate (KHCF; 99%), copper sulphate (97%), and *N*,*N*-methyl pyrrolidone (NMP; AR grade) were obtained from Merck. All the other solvents and the chemicals used were of analytical grade. Water obtained from Millipore-Q water purification system, with conductivity < 0.3 μS cm^{-1}, was used in all the experiments.

Synthesis of CuHCF–PES Composite

CuHCF powder was prepared by reacting the solution of copper sulphate (10 wt %) with KHCF solution (10 wt %) in the presence of PVA stabilizer (6 wt %) in aqueous medium. The copper sulphate solution was added drop wise into the KHCF solution, with continuous stirring. Brown-colored precipitate of CuHCF started to appear on mixing of the two solutions. PVA acts as a stabilizer in controlling the size of the CuHCF precipitates. The effect of PVA concentration on the particle size of the CuHCF precipitated was studied by particle size analyzer. It was observed that, in the absence of PVA, the size of the synthesized CuHCF was ~450 nm, and by varying PVA concentration, from 0 to 10 wt %, the size of CuHCF varied from 450 to 145 nm (figure not shown here). The precipitate was separated from the mother liquor by ultracentrifugation, and washed with water several times, to remove PVA and the leftover reactants. This precipitate was air-dried, to obtain a freely flowing fine brown powder. This powder was used to prepare sorbent–polymer composite beads. The synthesized CuHCF powder was dispersed in PES/NMP solution, to form homogenous slurry of appropriate viscosity. The polymeric composite beads, containing CuHCF, were produced by controlled precipitation of PES, present in the slurry, in the form of drops of required size in a suitable aqueous bath. The synthesized sorbent beads were used in the swollen state for thermogravimetric analysis (TGA) and sorption experiments, whereas infrared (IR), scanning electron microscopy (SEM), energy-dispersive X-ray fluorescence technique (EDXRF), and Brunauer–Emmett–Teller (BET) surface area studies were carried out with the air-dried composite beads.

Analytical Methods

Optical microscope images of the CuHCF–PES beads were recorded in a digital Blue QX5 computer microscope. SEM was used to observe microscopic morphology of the synthesized CuHCF–PES beads on AIS2100 SERON Tech. SEM from South Korea. Thermogravimetry (TG) was performed on Mettler Toledo (TG/DSC STAR^e System), at a heating rate of 10°C min^{-1} under N_2 atmospheres. X-ray diffraction (XRD) patterns were recorded with a Phillips X-ray diffractometer (Model: PW 1710 system, having a Cu Kα source ($\lambda = 0.15406$ nm)). EDXRF spectrum was recorded on EDXRF, Jordan Valley (EX3600M). IR spectra of the synthesized beads were recorded with IR spectrometer, IRAffinity1 in reflectance mode. Particle size analysis of the CuHCF particles was carried out by dynamic light scattering method, using VASCO$^{\gamma}$ particle size analyzer at 25°C (laser wavelength 658 nm). BET surface area of the RF–XAD beads was determined by N_2 adsorption–desorption measurement, using "SORPTOMATIC 1990" analyzer, from CE Instruments, Italy. Samples were outgassed at 100°C in vacuum before the measurement.

Sorption Studies

^{134}Cs radiotracer ($T_{1/2} = 2.06$ years; specific activity = 8.44 Ci mL^{-1}) was procured from the Board of Radiation and Isotope Technology, Mumbai, India. The solution was further diluted to the required concentrations, as and when required. The batch capacities of the resin were determined by shaking 0.5 g of CuHCF–PES resin with 5 mL of the $CsNO_3$ solution of appropriate concentration, containing cesium-134 as a radiotracer. The solution was stirred continuously, using a mechanical shaker, for 4 h, which was found to be sufficient for attaining equilibrium. However, for kinetic studies, the samples were equilibrated for different time intervals. After the equilibration, a small portion of the aqueous phase (0.5 mL) was separated, and taken for counting gamma activity. The gamma activity measurements were carried out in a well-type NaI (T1) [ECIL] detector, connected to a single-channel analyzer.

Equilibrium sorption capacity, q_e, was calculated using

$$q_e = \frac{(C_0 - C_e)V}{m} \quad (1)$$

where C_o is initial cesium ion concentration, C_e is equilibrium cesium ion concentration, V is volume of the cesium solution, and m is weight of the sorbent.

RESULTS AND DISCUSSION

Characterization of the Beads

The synthesized CuHCF–polymer composite beads were characterized, using XRD, IR, TGA, SEM, and BET surface area analysis techniques.

XRD and IR Studies. The crystal structure of the synthesized CuHCF was confirmed by XRD analysis (Figure 1). The XRD pattern of the synthesized CuHCF matches well with those previously reported[16] and indicates crystalline nature of the synthesized CuHCF powder. But, the presence of CuHCF in the beads was confirmed by EDXRF (Figure S1, Supporting Information).

Figure 2(a) represents the IR spectrum of CuHCF dry powder. Most relevant and characteristic bands in the samples fall at 595 cm^{-1} (medium), 3400–3600 cm^{-1} (broad), and 2090 cm^{-1} (strong). The last one corresponds to Fe(II)-CN stretch.[16] Low-intensity peak at 1610 cm^{-1} could be due to latice water. Figure 2(b,c) represents IR spectra of the blank PES and CuHCF–PES beads, respectively. On comparison between the IR spectra 2a,

Applied Polymer SCIENCE

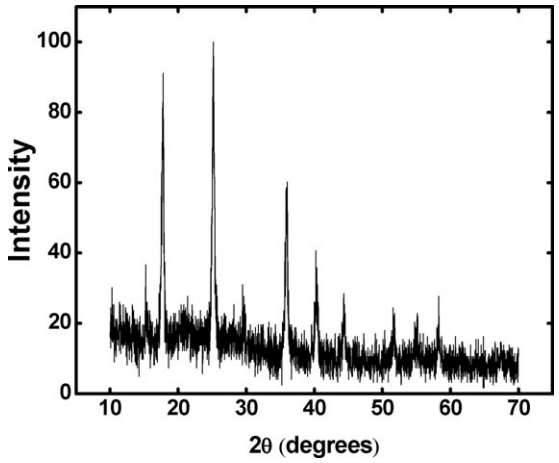

Figure 1. XRD pattern of the synthesized CuHCF powder.

2b, and 2c, it is observed that the characteristic peaks of the pure PES and diminished peaks of CuHCF powder are present in CuHCF–PES composite beads with some shift in vibrational frequencies due to the interaction between the components. The precipitation of the polymer starts at the surface of the beads, and slowly proceeds in the interior region, during the formation of the beads. Moreover, probability of loosing the fine CuHCF powder, present on the surface of the beads, is also more, when compared with that from the interior region. Both these factors may be responsible for the much lower loading of CuHCF at the surface of the synthesized beads when compared with that in the bulk. The IR spectra of all the samples were recorded in the reflectance mode, which gets signal transmitted mainly from the surface of the sample. This is probably the reason behind the observed diminished peak of 2090 cm^{-1} in the IR spectrum of the CuHCF–PES beads given in Figure 2(c), in spite of the overall higher loading of CuHCF in the beads.

Thermogravimetric analysis. Thermogravimetric analysis (TGA) of the synthesized beads was performed at a heating rate

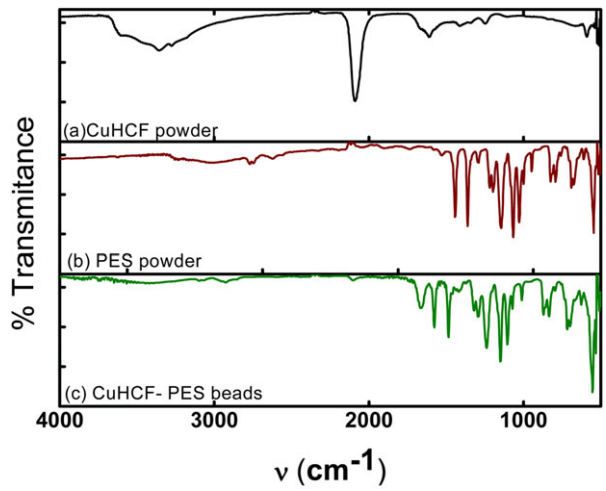

Figure 2. IR spectra of (a) CuHCF powder, (b) PES powder, and (c) CuHCF–PES beads. [Color figure can be viewed in the online issue, which is available at wileyonlinelibrary.com.]

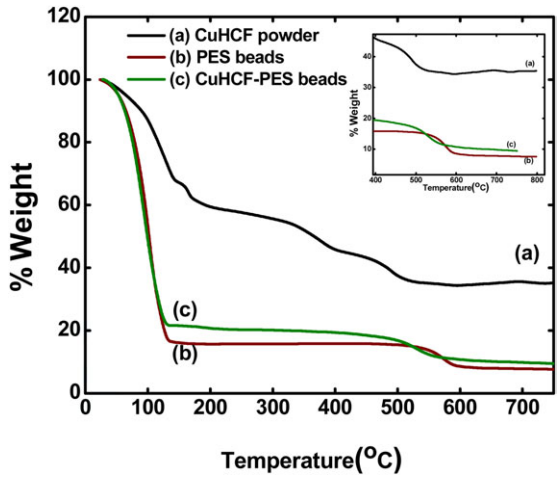

Figure 3. TGA profile of (a) CuHCF powder, (b) PES beads, and (c) CuHCF–PES beads. [Color figure can be viewed in the online issue, which is available at wileyonlinelibrary.com.]

of 10°C min^{-1} under nitrogen atmosphere, from ambient conditions upto 750°C. Figure 3 and inset figure show typical TGA profiles of the CuHCF powder, blank PES beads, and CuHCF–PES beads. The TGA profile of CuHCF powder [Figure 3(trace a)] can be divided into three main stages. The first stage is from 30 to 148°C, over which a mass loss of about 33% is observed due to dehydration.[17] The second stage, from 148 to 200°C, experiences an additional mass decrease of about 8%, due to loss of the last traces of water. The residual mass of 35% is left after 750°C. Figure 3(trace b) shows the TGA profile of the water-swollen blank PES beads. This profile consists of two steps. The first step, from 30 to 134°C, corresponds to weight loss (~83%) due to water loss. The degradation of PES starts at 522°C, whereas no change is seen in the weight after 625°C, and ~8% residual charred mass is obtained at the end of the sample run. Figure 3 (trace c) depicts the thermal degradation profile of the swollen CuHCF–PES beads, which is similar to that of blank PES beads, but the onset and completion of decomposition of PES have shifted to 490 and 593°C, respectively. The observed shift in the onset and completion of decomposition of PES in the CuHCF–PES beads could be due to the presence and simultaneous degradation of CuHCF particles along with the PES. The water content of these composite beads was determined to be ~79%. These results are summarized in Table I. These results show high-water content in the synthesized beads. It indicates high porosity of the composite beads and easy availability of the encapsulated CuHCF

Table I. Feed Loading of Sorbent and Moisture Content of the Synthesized CuHCF–PES Beads

Beads	Loading of the sorbent taken in the feed (%)	Water content (%)
CuHCF-PES	28.57	78.67
Blank PES	00.00	83.55

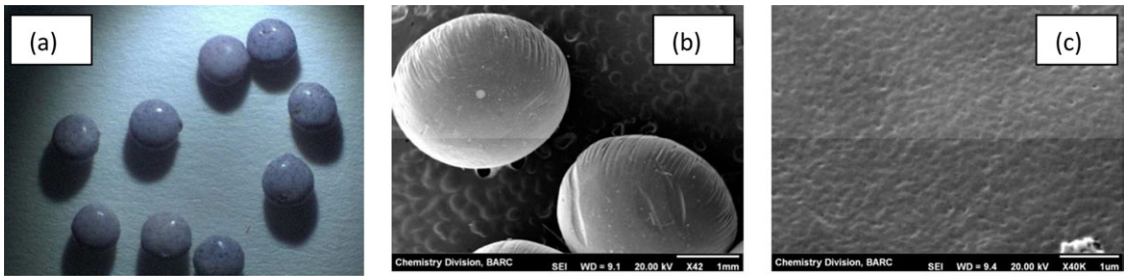

Figure 4. (a) Optical microscope and (b) and (c) SEM images of the CuHCF–PES beads and the surface of a bead, respectively. [Color figure can be viewed in the online issue, which is available at wileyonlinelibrary.com.]

sorbent. As synthesis of the composite beads was carried out using a feed mixture containing 28.6 wt % of CuHCF with respect to the polymer taken, the expected loading of CuHCF in the dry beads is 28.6 wt % or lower. On comparing all the TGA profiles, it was observed that after the thermal degradation of CuHCF powder up to 630°C, ~35% mass is left as residue, whereas after heating PES blank beads upto the same temperature, ~8% residue is obtained, and in the composite CuHCF–PES beads, only ~10% of the composite weight is obtained after heating up to 630°C (inset Figure 3). Based on these results and assuming average water content of the swollen beads as ~79%, the loading of the CuHCF powder on these beads was estimated to be ~28% of the dry CuHCF–PES composite weight, which is very close to that in the feed solution.

BET Surface Area. The specific surface area and the pore volume of the beads were determined by BET N_2 adsorption method. The nitrogen adsorption–desorption isotherms were measured at 77 K, after degassing the samples at 100°C, for 5 h. The surface area was found to be 479.1 $m^2\ g^{-1}$, and the pore volume was found to be 1.767 cc g^{-1}. This high value of the surface area could be due to the porous nature of the binding polymer. During the synthesis of the beads by phase inversion, the solvent (NMP) is exchanged by the water in the aqueous bath, and precipitation of the PES polymer starts. This process is very fast at the surface of the droplets, but as the polymer at the surface of the beads starts precipitating, the rate of exchange of NMP from inside the bead with water starts slowing down. Most of the extractant, that is, CuHCF particle remains embedded in the polymer matrix, whereas the slow exchange of solvent with water generates porosity in the beads. The surface area and pore volume measured are for the dried beads, but the actual sorption experiments are carried out using swollen beads. Therefore, the effective surface area and the pore volume of the swollen beads are expected to be still higher. The higher surface area value is indicative of the higher porosity, which will increase efficiency of the sorption process.

Optical Microscopy and SEM Studies. Figure 4 presents the optical microscopy and SEM images of the CuHCF–PES beads. From these images, it can be inferred that the beads can be synthesized in spherical shape, with good control over size. The outer surface of these beads is quite porous, as depicted in Figure 4(c). The porous nature of the beads is a desirable feature, as it will lead to better sorption properties.

Sorption Studies

Removal of cesium ions using CuHCF salt proceeds by two mechanisms, involving (a) incorporation of cesium and nitrate ions into the CuHCF matrix and (b) exchange of cesium ions with copper ions. Among these two, sorption of cesium and nitrate ion pair is the predominant step, which is a complex process, and includes at least two steps: (i) diffusion of Cs^+ and NO_3^- ion pairs into the solid and (ii) formation of a new phase. Loos-Neskovic and coworkers[18] proposed that copper occupies two different types of sites in CuHCF, one of the Cu(II) ion is in the position linked to Fe(II) through CN groups, and the second Cu(II) ion, not linked to the CN groups, partially occupies the interstitial positions, which seems to play a favorable role in the sorption. The ion pairs, Cs^+ and NO_3^-, are probably hosted in the vacancies of the structure, replacing the water molecules. The diffusion of the ion pairs is the main process, which occurs during the initial stages (<72 h) of the contact, whereas destruction of the old crystal structure and formation of a new phase is a very slow process and takes place only after several months of contact with cesium solution.[18] True ion exchange is also one of the processes taking place in the sorption system, but it plays very minor role. To get a deep insight into the sorption system, the sorption of cesium onto the synthesized beads was studied in detail, and sorption and kinetic data were analyzed, using various models. Batch experiments were carried out to investigate the effect of pH, Cs^+ ion concentration, and equilibration time, using $CsNO_3$ salt as a source of cesium ions and ^{134}Cs as a radiotracer.

Effect of pH. pH is one of the important factors in controlling the sorption of metal ions on a sorbent. The sorption of Cs^+ ions from aqueous solution of 25 mg L^{-1} concentration onto CuHCF–PES composite beads was studied in the pH range 1.8–12.2. The results, as depicted in Figure 5, reveal that the amount of cesium ions sorbed per unit mass of the sorbent at equilibrium (q_e) increases with the increase in pH till pH 9, and then, it decreases. The observed finding can be explained on the basis of the fact that, at low pH (<2) and at high pH (>10), the decomposition of the sorbent starts,[19] which explains the decrease in the Cs^+ uptake at higher pH. From these studies, it can be concluded that these beads work best for the removal of cesium ions in the pH range 5–9.

Effect of Cs^+ Ion Concentration. The sorption capacity of CuHCF–PES beads for cesium was determined by batch experiment, as a function of cesium ion concentration, at 27°C. It is observed that, q_e, the amount of cesium ions sorbed per unit

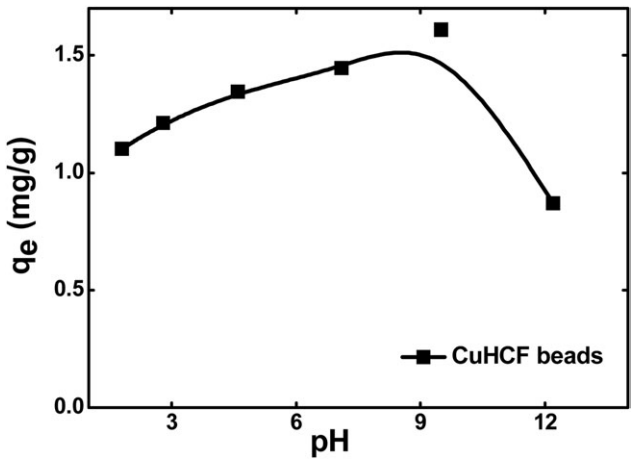

Figure 5. The effect of pH on the sorption of Cs^+ ions onto CuHCF–PES beads.

mass of the sorbent in milligram per gram increases with the increase in the concentration of Cs^+ ions, from 4 to 35 mg L^{-1} as shown in Figure 6(a). However, the percentage sorption decreases with the increase in the concentration of Cs^+ ions, as shown in Figure 6(b). The initial concentration provides an important driving force to overcome all the mass transfer resistances to the cesium ions between the aqueous and the solid phases. Therefore, a higher initial cesium ion concentration will enhance the sorption process. It is observed that the q_e value for sorption of cesium ions increases with the increase in the initial cesium ion concentration, and then, starts attaining saturation after a concentration of 25 mg L^{-1}. This can be explained by the fact that, with the increase in the concentration, the metal ion uptake by the sorbent is initially linear, because enough number of active sites are available, but at higher concentration it starts saturating, as competition for the available active sites intensifies.

Sorption Isotherms. Because the quantity of the metal ions sorbed by the sorbent is a function of both the metal ion concentration and the temperature, the amount of metal ions sorbed was determined as a function of the initial metal ion concentration at a constant temperature, and the sorption equilibrium data were fitted into various isotherm models. Sorption isotherms are basically used to determine important sorption parameters, which can be used for the purpose of sorption design. The sorption equation parameters and the underlying thermodynamic assumptions describe the surface properties and affinities of the sorbent, and how the solute interacts with the sorbent. The experimental isotherm data are usually analyzed by Langmuir, Freundlich, Temkin, and Dubinin-Redushkevich isotherms.[20–22] The linearized forms of the different sorption isotherm models are given below.

$$\text{Langmuir isotherm}: \frac{1}{q_e} = \frac{1}{q_m} + \frac{1}{K_L q_m C_e} \quad (2)$$

$$\text{Freundlich isotherm}: \log q_e = \log K_F + \frac{1}{n}\log C_e \quad (3)$$

$$\text{Temkin isotherm}: q_e = \frac{RT}{b}\ln K_T + \frac{RT}{b}\ln(C_e) \quad (4)$$

$$\text{Dubinin-Redushkevich isotherm}: \ln q_e = \ln q_m - K_{DR}\varepsilon^2 \quad (5)$$

where $\varepsilon = RT\ln(C_o - C_e)$ and q_m is the theoretical maximum monolayer capacity, K_L, K_F, and n, K_T and b, and K_{DR}, respectively, are Langmuir, Freundlich, Temkin, and the D–R model constants, and ε is the Polanyi potential.

The experimental sorption data were fitted into the linearized forms of the sorption isotherm models, and from the different plots, the respective sorption isotherm parameters were determined. The values of the sorption isotherm parameters are given in Table II. Figure 7 depicts the Langmuir isotherm plot for sorption of cesium ions onto the synthesized beads. The plot of $1/q_e$ versus $1/C_e$ is a straight line. The values of q_m and K_L can be calculated from the intercept and the slope, respectively. The value of correlation coefficient R^2 is 0.998, which indicates a good correlation between the experimental data and the Langmuir sorption model. The maximum sorption capacity of CuHCF beads for Cs^+ ions is determined to be 1.56 mg g^{-1} of the resin. The sorption coefficient, K_L, is determined to be 0.851 L mg^{-1}. The favorability of sorption of Cs^+ ions onto the CuHCF–PES beads can be expressed in terms of a dimensionless constant, (R_L), called separation factor, using the essential features of the Langmuir isotherm, as given below:

$$R_L = 1/(1 + K_L C_o) \quad (6)$$

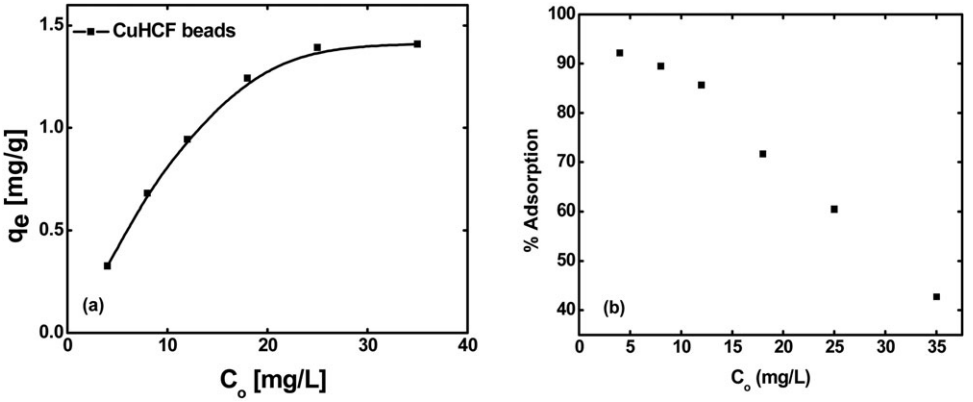

Figure 6. Effect of the initial metal ion concentration on the sorption of Cs^+ ions onto CuHCF–PES beads.

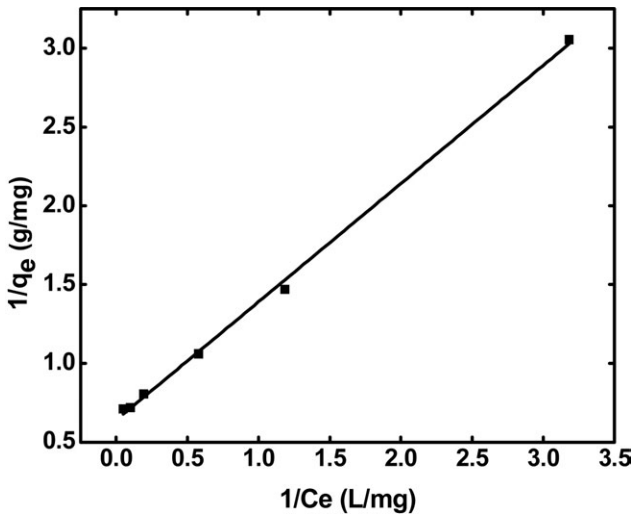

Figure 7. Langmuir isotherm plot for sorption of Cs^+ ions onto CuHCF–PES beads at 300 K.

The calculated value of R_L lies between 0.54 and 0.02, which indicates that the CuHCF beads are good sorbents for Cs^+ ions, and the sorption process is favorable for the efficient removal of Cs^+ ions from aqueous waste solutions. The data were analyzed by applying Freundlich isotherm, by plotting log (q_e) versus log (C_e), as shown in Figure S2 (Supporting Information). From the slope and the intercept of this straight line, respectively, the values of $1/n$ and K_F are determined. The correlation coefficient R^2 for this plot is 0.846, which suggests that the correlation between the experimental data and the Freundlich isotherm model is not as good as that of the Langmuir sorption model. The plot of the q_e versus ln C_e is a straight line, with the correlation coefficient R^2 value of 0.957 (Figure S3, Supporting Information). It shows that the experimental equilibrium data are in good correlation with the Temkin model too. The Temkin constant, b, is determined to be 9.21 kJ mol^{-1}. The typical range of the binding energy for ion exchange mechanism is 8–16 kJ mol^{-1}.[22] The value of b obtained in the present study indicates weak interaction between the sorbate and the sorbent. The experimental data were also analyzed in terms of D–R isotherm model. Figure S4 (Supporting Information) shows that the plot of ln (q_e) versus ε^2 for the sorption of cesium ions onto CuHCF–PS beads is a straight line, with a correlation coefficient R^2 of 0.874. From the intercept and the slope of the plot, the values of K_{DR} (also known as the porosity factor, for the CuHCF beads toward Cs^+ ions) and q_m of the CuHCF beads for Cs^+ ions are determined to be 0.037 and 1.748 mg g^{-1}, respectively. The porosity factor less than unity implies that the synthesized beads consist of fine micropores and indicate surface heterogeneity.

Effect of Equilibration Time. The effect of equilibration time on the sorption of cesium ions from aqueous solutions onto the CuHCF–PES beads, at neutral pH, is presented in Figure 8. The sorption increases with the increase in contact time. The uptake of Cs^+ ions is rapid in the first 30 min, and then, it becomes slow until a state of equilibrium is reached. In the first 30 min, nearly 48–70% of the total metal ion uptake appears to have taken place, depending on the initial metal ion concentration taken. The initial rapid phase is due to the abundant availability of the active sites in the initial stage. Later on, the process becomes relatively slower, and equilibrium conditions are reached in 120–240 min. At this point, the amount of the cesium ions being sorbed onto the sorbent is in dynamic equilibrium with the amount of the cesium ions desorbing from the sorbent. The time required to attain this state of equilibrium is termed as the equilibrium time, and the amount of cesium ions sorbed at the equilibrium time reflects the maximum sorption capacity of the sorbent under those operating conditions. Therefore, all the further batch experiments were carried out at 240 min of equilibration time.

Kinetic Modeling. Sorption kinetics studies are important from the view point of both understanding the sorption process and applications thereof. To investigate the sorption of cesium ions onto the CuHCF–PES beads, different kinetic models have been used. The pseudo-first-order model and pseudo-second-order kinetic models can be described by the following equations[23,24]:

$$\text{Pseudo first-order kinetic model}: \frac{dq_t}{dt} = k_1(q_e - q_t) \quad (7)$$

$$\text{Pseudo second-order kinetic model}: \frac{dq_t}{dt} = k_2(q_e - q_t)^2 \quad (8)$$

where q_t is the amount of the cesium ions adsorbed at time t, and k_1 and k_2 are the pseudo first-order and pseudo second-order rate constants, respectively. After integration and applying the boundary conditions, at $t = 0$ and $q_t = 0$, the linearized forms of the two models can be written as follows:

$$\text{Pseudo first-order kinetic model}: \log(q_e - q_t) = \log(q_e) - \frac{k_1}{2.303}\, t \quad (9)$$

$$\text{Pseudo second-order kinetic model}: \frac{t}{q_t} = \frac{1}{k_2 q_e^2} + \frac{1}{q_e}\, t \quad (10)$$

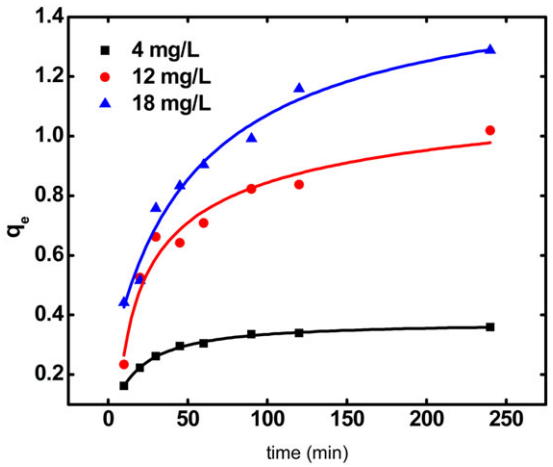

Figure 8. The effect of equilibration time on the sorption of Cs^+ ions onto CuHCF–PES beads at different initial concentrations. [Color figure can be viewed in the online issue, which is available at wileyonlinelibrary.com.]

Applied Polymer SCIENCE

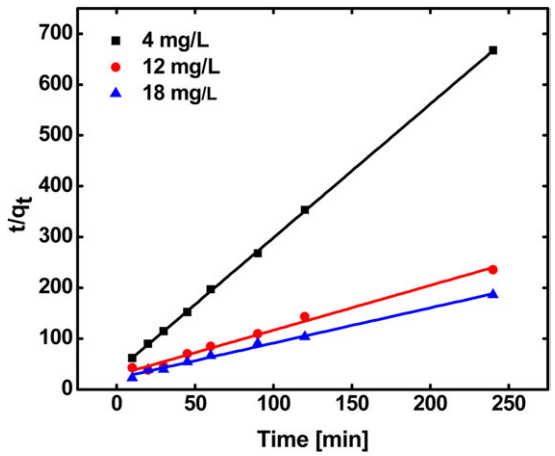

Figure 9. Pseudo second-order plots for the Cs^+ ion sorption onto CuHCF–PES beads at three different initial concentrations of Cs^+ ions. [Color figure can be viewed in the online issue, which is available at wileyonlinelibrary.com.]

The values of k_1 and q_e for pseudo first-order kinetics can be determined from the slope and intercept, respectively, of the straight line plot of log $(q_e - q_t)$ versus t (Figure S5, Supporting Information). Similarly, the pseudo second-order rate constants, k_2 and q_e, can be determined from the t/q_t versus t plot (Figure 9). The values of k_2, and corresponding correlation coefficients (R^2), along with the theoretically determined values of q_e, from pseudo second-order rate models, are given in Table III. The R^2 values for the pseudo-first-order model are quite small when compared with that for the pseudo second-order rate model. Moreover, the q_e values determined from the pseudo first-order rate model do not match with the corresponding experimental values, whereas the q_e values determined from pseudo second-order rate model are in close agreement with the experimentally determined q_e values. Therefore, it can be concluded that the sorption of cesium ions onto the sorbent beads follows pseudo second-order kinetics for the entire period of time and for all the studied initial concentrations. The amount of the metal ions sorbed on the surface and the equilibrium metal ion concentration affect the pseudo second-order reaction rate significantly. The rate is directly proportional to the number of the active sites on the surface of the sorbent. From the results shown in Table III, it is clear that k_2 decreases with the increase in the initial Cs^+ ion concentration. The values of q_e obtained from kinetics match very well with the experimental values, and the observed higher value of R^2 suggests that the model can be applied to the sorption process in the entire studied concentration range.

Mechanism. The transfer of the sorbate from the solution phase onto the surface of the sorbent particles is a gradual process, and completes after several steps, such as film or external diffusion, surface diffusion, pore diffusion, and sorption on the pore surface. The overall sorption process may be controlled by one or a combination of more than one steps. From Figure 10, it is clear that, with increase in the contact time, there is an increase in the sorption capacity of CuHCF beads for Cs^+ ions, which indicates that the sorption process can be intraparticle diffusion-controlled. Therefore, such a possibility was explored by using the intraparticle diffusion model. This model is represented by the following equation[25]:

$$q_t = k_{id} t^{\frac{1}{2}} + I \tag{11}$$

where k_{id} is the intraparticle diffusion rate parameter and I (mg g^{-1}) is a constant that gives idea about the thickness of the boundary layer. If the intraparticle diffusion occurs, then the plot of q_t versus $t^{1/2}$ will be linear, and, if this straight line passes through origin, then only the intraparticle diffusion is the rate controlling step; otherwise, some other mechanism may also be involved.

As shown in Figure 10, the plot of q_t versus $t^{1/2}$ is a multilinear plot, indicating that the sorption process consists of multiple stages. In the first stage, the external surface of the sorbent gets saturated, indicated by the small portion of the curve with steep slope. Then, the stage of intraparticle diffusion control starts, indicated by the portion of the curve with gentle slope. The final equilibrium process, leading to equilibrium, starts after that, and is comparatively slow due to very low concentration of the sorbate left in the solution. Generally, the slope of stage II gives the intraparticle diffusion rate constant k_{id}, and its value for the studied system increases with the increase in the initial cesium ion concentration from 4 to 18 mg L^{-1}. The I value also increases with the increase in the initial metal ion concentration. To further confirm whether the sorption proceeds via film diffusion or intraparticle diffusion mechanism, the kinetic data were analyzed using the kinetic expression given by Boyd et al.[26]

$$F(t) = 1 - \frac{6}{\pi^2}\sum_{n=1}^{\infty}\frac{1}{n^2}\exp\left(-\frac{D_i\pi^2 tn^2}{r_o^2}\right). \tag{12}$$

$$F(t) = 1 - \frac{6}{\pi^2}\sum_{n=1}^{\infty}\frac{1}{n^2}\exp\left(-n^2 Bt\right) \tag{13}$$

Table II. Isotherm Constants of the Different Models for Sorption of cesium ions onto CuHCF–PES Beads

Isotherm model	Parameters	
Langmuir	q_m	1.562 mg/g
	K_L	0.851 L/mg
	R^2	0.998
Freundlich	K_F	0.633
	$1/n$	0.334
	R^2	0.846
Temkin	b	9.210 kJ/mol
	K_T	14.450
	R^2	0.957
D–R	q_D	1.748 (mg/g)
	K_{DR}	0.037
	R^2	0.874

Table III. Kinetic Parameters for the Sorption of Cesium Ions onto CuHCF–PES Resin at Different Initial Cesium Ion Concentrations

Kinetic model	Parameters	C_o = 4 mg/L	C_o = 12 mg/L	C_o = 18 mg/L
Pseudo first-order	k_1 (min^{-1})	0.021	0.042	0.024
	q_e (mg/g)	0.198	0.907	0.946
	R^2	0.947	0.849	0.952
Pseudo second-order	k_2 (g mg^{-1} min^{-1})	0.193	0.039	0.022
	q_e (mg/g)	0.380	1.132	1.441
	R^2	0.989	0.999	0.993
Intraparticle diffusion	k_{id} (g mg^{-1} $min^{-1/2}$)	0.015	0.065	0.056
	I (mg/g)	0.191	0.204	0.461
	R^2	0.946	0.999	0.986

where $B = \pi^2 D_i / r_0^2$ and F is the fractional attainment of equilibrium, that is, the ratio of the solute sorbed at time, t, to that at equilibrium ($F = q_t/q_e$), D_i the effective diffusion coefficient of metal ion, r_o the radius of the sorbent, and n is an integer.

Solutions to the eq. (13), depending on the value of F, are given in eqs. (14) and (15).[27]

$$Bt = 2\pi - \frac{\pi^2 F}{3} = 2\pi\left(1 - \frac{\pi F}{3}\right)^{1/2} \quad (14)$$

$$Bt = -0.4977 - \ln(1 - F) \quad (15)$$

Thus, the value of Bt can be calculated for each value of F, using eq. (14) for F values up to 0.85 and eq. (15) for higher F values.[27] The calculated Bt values were plotted against time (Figure S6, Supporting Information). The linearity of this plot provides useful information to distinguish between the film diffusion and the intraparticle diffusion of sorption.[28] A straight line passing through the origin is indicative of sorption process only governed by intraparticle–diffusion mechanism; otherwise, it is governed by film diffusion.[29] In the present case, the plots are scattered, and do not pass through the origin, indicating the complex nature of the sorption process and film diffusion as the rate-determining step.

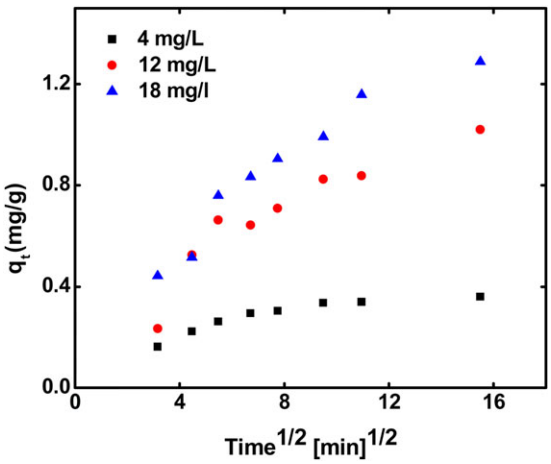

Figure 10. Intraparticle diffusion plot for the Cs^+ ion sorption onto CuHCF–PES beads at three different initial concentrations of Cs^+ ions. [Color figure can be viewed in the online issue, which is available at wileyonlinelibrary.com.]

CONCLUSION

The present study shows that the CuHCF–PES composite beads can be easily synthesized by phase-inversion technique, and can be used as a sorbent for the removal of cesium ions from waste water. The surface area of the synthesized composite is 479 m^2 g^{-1}. The equilibrium sorption data are analyzed, using various sorption isotherm models, and the data are found to follow Langmuir isotherm the best, confirming the monolayer coverage of cesium ions onto the composite beads. From Temkin model, it is inferred that the sorption of cesium ions onto the beads is a spontaneous process. Among the different kinetic equations applied, the kinetics data fit well into the pseudo-second-order rate model. Analysis of the mechanistic steps involved in the sorption process reveals the complex nature of the sorption. From intraparticle diffusion model, it can be inferred that the process mechanism is complex and consists of both film diffusion and intraparticle diffusion. The synthesized beads show good stability and sorption capacity, and can be used for the removal of cesium ions from the low-level liquid waste efficiently in batch mode of operation.

ACKNOWLEDGMENTS

The author, Charu Dwivedi, is grateful to BRNS, Department of Atomic Energy, for awarding research fellowship. The authors are thankful to Mr. J. Nuwad and Dr. C.G.S. Pillai for SEM experiments, and Mr. T. V. V. Rao, Dr. K. T. Pillai, and Dr. S. K. Mukerjee for BET surface area measurement. The authors also acknowledge Dr. T. Mukherjee and Dr. S.K. Sarkar for their encouragement during the course of the study.

REFERENCES

1. Zhang, F.-S.; Nriagu, J. O.; Itoh, H. *Water Res.* **2005**, *39*, 389.
2. Yavuz, E.; Senkal, B. F.; Bicak, N. *React. Funct. Polym.* **2005**, *65*, 121.
3. Tonle, I. K.; Ngameni, E.; Njopwouo, D.; Carteret, C.; Walcarius, A. *Phys. Chem. Chem. Phys.* **2003**, *5*, 4951.
4. Walcarius, A.; Delacôte, C. *Anal. Chim. Acta* **2005**, *547*, 3.

5. Vatutsina, O. M.; Soldatov, V. S.; Sokolova, V. I.; Johann, J.; Bissen, M.; Weissenbacher, A. *React. Funct. Polym.* **2007**, *67*, 184.
6. Klisuranov, G. S.; Gradev, G.; Stefanova, I.; Milusheva, A. Proceedings of the IAEA-TECDOC-675, Vienna, Austria, **1992**; p 121.
7. Nilchi, A.; Maragheh, M. G.; Khanchi, A. R. *Separ. Sci. Technol.* **1999**, *34*, 1833.
8. Möller, T.; Harjula, R.; Paajanen, A. *Separ. Sci. Technol.* **2003**, *38*, 2995.
9. Mishra, S. P.; Vijaya. *Separ. Purif. Technol.* **2007**, *54*, 10.
10. Inan, S.; Altaş, Y. *Separ. Sci. Technol.* **2010**, *45*, 269.
11. Ayers, J. B.; Waggoner, W. H. *J. Inorg. Nucl. Chem.* **1971**, *33*, 721.
12. Hendrickson, W. F.; Riel, G. K. *Health Phys.* **1975**, *2*, 817.
13. Ishfaq, M. M.; Karim, H. M. A.; Khan, M. A. *J. Radioanal. Nucl. Chem.* **1992**, *159*, 335.
14. Loewenschuss, H. *Radioact. Waste Manag.* **1982**, *2*, 327.
15. Tusa, E. H.; Paavola, A.; Harjula, R.; Lehto, J. *Proc. Symp. Waste Manag.* **1993**, *2*, 1687.
16. Byun, I. S.; Kim, I. C.; Seo, J. W. *J. Appl. Polym. Sci.* **2000**, *76*, 787.
17. Singh, I. J.; Misra, B. M. *Separ. Sci. Technol.* **1996**, *31*, 1695.
18. Ayrault, S.; Jimenez, B.; Garnier, E.; Fedoroff, M.; Jones, D. J.; Loos-Neskovic, C. *J. Solid State Chem.* **1998**, *141*, 475.
19. Collins, J. L.; Egan, B. Z.; Anderson, K. K.; Chase, C. W.; Mrochek, J. E.; Bell, J. T.; Jernigan, G. E. Technical Report ORNL/TM-12938, Oak Ridge National Laboratory, Oak Ridge, TN, **1995**.
20. Hall, K. R.; Eagleton, L. C.; Acrivos, A.; Vermeulen, T. *Ind. Eng. Chem. Fundam.* **1966**, *5*, 212.
21. Das, D.; Das, N.; Mathew, L. *J. Hazard. Mater.* **2010**, *184*, 765.
22. Sheha, R. R.; Metwally, E. *J. Hazard. Mater.* **2007**, *143*, 354.
23. Ho, Y. S. *Scientometrics* **2004**, *59*, 171.
24. Ho, Y. S. *Water Res.* **2006**, *40*, 119.
25. Ho, Y. S.; McKay, G. *Can. J. Chem. Eng.* **1998**, *76*, 822.
26. Boyd, G. E.; Adamson, A. W.; Myers, L. S., Jr. *J. Am. Chem. Soc.* **1947**, *69*, 2836.
27. Reichenberg, D. *J. Am. Chem. Soc.* **1953**, *75*, 589.
28. Singh, B. K.; Rawat, N. S. *J. Chem. Technol. Biotechnol.* **1994**, *61*, 57.
29. Sankar, M.; Sekaran, G.; Sadulla, S.; Ramasami, T. *J. Chem. Technol. Biotechnol.* **1999**, *74*, 337.